Self-consistent axial modeling of surface-wave-produced discharges at low and intermediate pressures

Ts. Petrova,[1] E. Benova,[2] G. Petrov,[3] and I. Zhelyazkov[1,*]
[1]*Faculty of Physics, Sofia University, BG-1164 Sofia, Bulgaria*
[2]*Department of Physics, Institute for Foreign Students, BG-1111 Sofia, Bulgaria*
[3]*Institute of Solid State Physics, Bulgarian Academy of Sciences, BG-1784 Sofia, Bulgaria*
(Received 19 November 1998)

A model for description of the axial structure of a surface-wave-produced and -sustained plasma based on numerical calculation of a complete set of electrodynamic and kinetic equations is presented. The model includes a self-consistent solution to the electron Boltzmann equation, a set of particle balance equations for electrons, excited atoms, atomic and molecular ions, as well as Maxwell's equations with appropriate boundary conditions. A gas thermal balance equation is used to predict the neutral gas temperature self-consistently. Precise calculations of discharge characteristics of an argon plasma column sustained by an azimuthally symmetric surface wave at low and intermediate gas pressures have been performed. A comparison with available experimental data is done in order to test the validity of the model. [S1063-651X(99)00107-5]

PACS number(s): 52.25.Dg, 52.50.Dg, 52.80.Pi

I. INTRODUCTION

Over the past two decades surface-wave (SW) discharges have been systematically investigated both experimentally and theoretically. Due to the broad range of operating conditions of these discharges, they have received many technological applications such as surface treatments, laser and spectroscopic sources, lamp technology, elemental analysis, etc.

Several theoretical works on SW discharges at different operating conditions and various configurations have been performed by Glaude *et al.* [1], Ferreira [2], Zakrzewski [3], Mateev *et al.* [4], Zhelyazkov *et al.* [5], Ferreira [6], Boisse-Laporte *et al.* [7], Ferreira and Moisan [8], Zhelyazkov and Benova [9], Ferreira [10,11], Benova and Zhelyazkov [12], Kortshagen *et al.* [13], Sá *et al.* [14], Aliev *et al.* [15], Ferreira *et al.* [16], Zhelyazkov and Atanassov [17], and Zhang *et al.* [18].

The fact that the wave propagates along a plasma column sustained by the wave itself makes the problem rather complex since it is necessary to analyze the plasma behavior in two aspects: wave and gas-discharge ones. The first aspect based on the electrodynamics permits a full description of the wave propagation which does not depend on the type of the wave launcher (surfatron [19], surfaguide [20], Ro-box [21], transmission-line and antenna applicator [22]). It allows studying of various configurations of the waveguiding structure (the role of the dielectric container [9] and the metal enclosure [12]), different modes of the electromagnetic wave (azimuthally symmetric and dipolar [23–25]), and the influence of an external axial magnetic field [26–33]. The second aspect, based on a kinetic description, stresses the elementary processes and enables studying plasmas at different gas-discharge conditions: gas pressures from 1 mTorr to a few atmospheres, tube diameters from 1 mm to several centimeters, and in a wide range of applied frequencies—from a few hundred kilohertz to 10 GHz. A novel element in the modeling is the inclusion of a gas energy balance in order to predict the gas temperature which, as it turns out, changes along the column length.

The first model for a theoretical description of the axial structure of a plasma column sustained by an azimuthally symmetric SW was proposed by Glaude *et al.* [1]. Later on, this method was significantly improved by Ferreira [2] including a kinetic treatment of the problem. The most detailed model for an argon plasma column at low pressures has been developed by Sá *et al.* [14]. In all these models the determination of both the axial plasma density and wave power is based on calculating the wave attenuation coefficient (following different kinds of approximations) and the mean power θ required for sustaining an electron-ion pair in the discharge.

Another approach for studying the electrodynamics of SW discharges has been suggested by Zhelyazkov *et al.* [5] and by Aliev *et al.* [15]. The model consists of solving three equations, namely the local wave dispersion relation, the wave energy balance equation, and the electron energy balance equation, which yields a relation between the local absorbed wave power and the electron density. While the first two equations are nondisputable from a physical point of view, the third relation has been somehow artificially postulated. Despite the fact that it is assumed to depend on the discharge conditions, in fact it represents the discharge kinetics only qualitatively. Since the latter strongly influences the wave and plasma characteristics, that relation needs substantial improvement. Recently, a self-consistent model for an argon plasma column at intermediate pressures has been developed [34]. In that model the dependence of the local absorbed wave power on the electron density has been determined from the electron energy balance equation considering an appropriate energy level structure of the argon atom and assuming a Maxwellian electron energy distribution function (EEDF). However, systematic investigations of the EEDF for microwave discharges provided by Kortshagen [35] showed

*Electronic address: izh@phys.uni-sofia.bg

that the EEDF is very far from Maxwellian especially for plasmas with a low degree of ionization.

In this paper, a new axial self-consistent model of an argon plasma column sustained by a traveling azimuthally symmetric electromagnetic wave is presented. The model is based on a simultaneous solving of the electron energy and electron Boltzmann equations, a set of particle balance equations for electrons, excited argon atoms, atomic and molecular ions, the local dispersion relation, and the wave energy balance equation. The relation between the absorbed wave power and the electron density is derived from a detailed collisional-radiative model for argon and from a numerical calculation of the homogeneous EEDF. Compared with [34], where the EEDF was considered to be Maxwellian, now the kinetic part of the model is substantially improved. Thus, the limited accuracy and applicability of the former model are overcome and the new model provides an accurate description of both the axial plasma kinetic and wave characteristics in a wide range of discharge conditions. It also yields the spatial distribution of gas temperature.

The organization of the paper is as follows: in the next section a detailed description of the collisional-radiative model is given. A comparison between the model and the available experimental results as well as a theoretical investigation of the influence of the gas pressure on discharge characteristics is reported in the third section. In the conclusion several advantages and disadvantages of the model have been pointed out and its future improvement is discussed.

II. DESCRIPTION OF THE MODEL

A. General aspects

Most of the theoretical models of SW discharges consist of two independent parts: kinetic and electrodynamic. Some of them include only the electrodynamics—the gas-discharge information (collision frequency and the mean power θ) is usually ''imported'' from outside. It is the purpose of this model to couple these parts in order to develop a unique description of the axial properties of the discharge. From a complete set of equations given in the second (B) and the third (C) parts of this section and following the numerical procedure described in Sec. II D, we can derive self-consistently all discharge and wave characteristics, namely the EEDF, the electron density, the mean electron energy, the effective electron-neutral collision frequency for momentum transfer ν_{eff}, the mean power θ required for sustaining an electron-ion pair in the discharge, the densities of excited atoms, atomic and molecular ions, the wave number k, the wave power S, all the wave field components, and the gas temperature T_g as a function of the axial coordinate z. The model has been applied to an argon plasma column at various operating parameters: gas pressure, tube radius, input wave power, and angular frequency ω.

B. Kinetic part

1. Electron kinetics

It is well known that a detailed modeling of a SW plasma requires the knowledge of the EEDF, which determines the electron transport parameters, the rates of elementary processes, and several other key quantities such as the effective frequency for momentum transfer ν_{eff} and θ [8]. In the most models, two limiting cases have often been considered: low electron densities for which the Coulomb interactions can be neglected and the case of sufficiently high electron densities so that a Maxwellian distribution can be assumed. In argon plasmas the EEDF usually strongly differs from Maxwellian and for the theoretical treatment of SW discharges it is of major importance to determine it precisely. In our case the derivation of the EEDF is crucial since further on it is coupled with the electrodynamic equations. Any assumption for the EEDF (be it analytical expression, Maxwellian, or Druyvesteyn-type function) leads to substantial errors in the electron transport properties and consequently in the electrodynamic part.

In gas-discharge plasmas a strict treatment of electron kinetics has to include a wide spectrum of collisional processes such as elastic collisions (electron-electron, electron-ion, and electron-atom) and several inelastic collisions (excitation, ionization), three-body collisions (which are responsible for the molecular ion formation), recombination, ambipolar diffusion, radiative processes (taking into account the imprisonment of radiation), as well as the impact of the effective electric field

$$E_{\mathrm{eff}}=\frac{E_0}{\sqrt{2}}\frac{\nu_c(u)}{\sqrt{\nu_c^2(u)+\omega^2}}.$$

Here ν_c is the electron-neutral collision frequency for momentum transfer and E_0 is the radially averaged wave electric field. Note that the effective field E_{eff} is energy dependent via ν_c. The denotation $E_0/\sqrt{2}$ means a steady-state discharge maintenance root-mean-square electric field. It is a parameter in the numerical code determined self-consistently from the electron particle balance equation. Following the condition for stationarity given by Winkler *et al.* [36], namely that ω is larger than the energy relaxation frequency, the EEDF may be regarded as time independent.

It is of major importance to choose appropriate excited states of the atom and charged particles involved in the discharge. We consider the $\mathrm{Ar}(3p^5 4s)$ configuration in which the four levels (two metastable and two resonance) are treated separately and one lumped $\mathrm{Ar}(3p^5 4p)$ block of levels. This choice enables an accurate description of both the electron and heavy particle kinetics at low and intermediate gas pressures. An energy level diagram of the argon atom is shown in Fig. 1.

Several ionization processes are involved in the model: direct ionization, stepwise ionization, Penning, and associative ionization. All these processes are considered as processes in which electrons are created. It is assumed that after an ionization event the primary and the ejected electrons share the remaining energy. It has been shown that such an approach ensures sufficient accuracy in calculating the EEDF [37]. The loss of electrons is through recombination and diffusion processes. Both dissociative and three-body recombination are considered. The diffusion loss term is described by the generalized diffusion frequency $\nu_{\mathrm{diff}}=(\mu/R)^2 D_a$, where D_a is the ambipolar diffusion coefficient and μ is a number, usually between 2 and 3, depending on the gas-discharge conditions. For a Bessel radial profile of charged

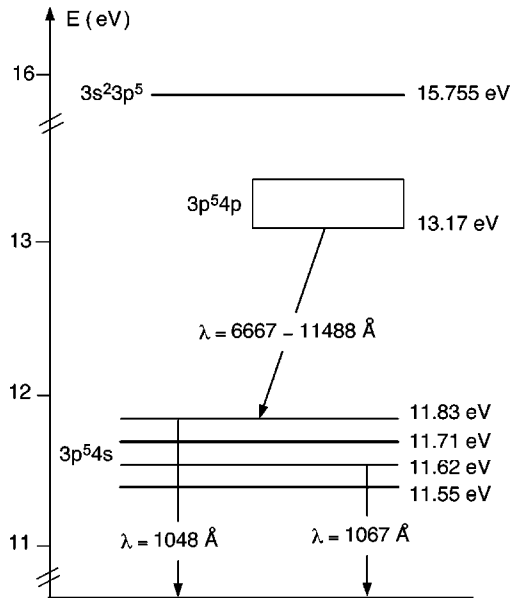

FIG. 1. Energy level diagram of the argon atom.

particles $\mu=2.405$, although the value of μ is usually taken to be less than 2.405 in order to avoid the wave resonance absorption near the tube wall [38].

The treatment of the homogeneous electron Boltzmann equation is based on the conventional two-term Legendre polynomial expansion assuming a quasistationary approximation of the anisotropic part of the distribution. The homogeneous electron Boltzmann equation is written down in the form [35]

$$\frac{dF}{du}=-\sum_j (u+U_j^{\mathrm{exc}})N_jQ_j^{\mathrm{exc}}(u+U_j^{\mathrm{exc}})f_0(u+U_j^{\mathrm{exc}}) -4\sum_{i=0}^{5}(2u+U_i^{\mathrm{ion}})N_iQ_i^{\mathrm{ion}}(2u+U_j^{\mathrm{ion}})f_0(2u+U_j^{\mathrm{ion}}), \tag{1}$$

where N_j is the population of the lower level for each of the excitation events involved and Q_j^{exc} and U_j^{exc} are the corresponding collision cross section and energy threshold. N_i is the population of the level from which the ionization occurs. Q_i^{ion} and U_i^{ion} are the appropriate collision cross section and energy threshold, respectively. F is the total electron flux in energy space being the sum of the flux driven by the applied wave electric field and the fluxes from elastic and inelastic collisions. In addition, it contains terms describing the diffusion and several recombination processes as well as Penning and associative ionization.

The EEDF has been calculated using conventional numerical technique based on finite difference approach. The numerical scheme employed has fast convergence. The inscattering and Coulomb terms are treated iteratively [39]. At a sufficiently high kinetic energy u_∞ the EEDF becomes negligibly small and $f_0(u_\infty)=0$ is used as a boundary condition. Here, f_0 is normalized according to

$$\int_0^\infty f_0(u)u^{1/2}du=1.$$

The EEDF obtained satisfies both the particle and energy balance equations for electrons as well as the balance equations for heavy particles considered.

The electron energy balance equation yields detailed information on how the power absorbed by electrons is dissipated in collisions. It can be derived by multiplying the electron Boltzmann equation by the kinetic energy and then integrating over the entire energy space. The energy balance for electrons can be conveniently written down in the form

$$\theta\equiv\frac{1}{2}(n_e)^{-1}\mathrm{Re}(\sigma)E_0^2 =\frac{2m}{M}\langle u\,\nu_{\mathrm{ea}}\rangle+\frac{2m}{M}\langle u\,\nu_{\mathrm{ei}}\rangle+\nu_{\mathrm{diff}}\langle u\rangle+\sum_k U_k\langle\nu_k\rangle +\sum_k \nu_k^{\mathrm{rec}}\langle u\rangle-\sum_k\frac{c_k^{\mathrm{Pen}}N_k^2}{n_e}\Delta U^{\mathrm{Pen}}, \tag{2}$$

where the angular brackets $\langle\ \rangle$ denote energy averaged values, ν_{ea} is the elastic electron-atom collision frequency, ν_{ei} the elastic electron-ion collision frequency, ν_{diff} the ambipolar diffusion frequency, and ν^{rec} being the dissociative or electron-ion recombination frequency. The inelastic processes (excitation and ionization) are with frequencies ν_k—k being the number of the process with corresponding threshold energy U_k. The Penning ionization process is described by the Penning ionization rate constant c_k^{Pen} with N_k being the population of either the $^3P_2$ or $^3P_0$ state and ΔU^{Pen} is the energy gain per collision. The terms on the right-hand side represent the mean elastic and inelastic energy losses per electron whose sum is equal to the energy gain from the wave electric field (the left-hand side of the equation). Here $\mathrm{Re}(\sigma)$ is the real part of the complex electron conductivity

$$\sigma=-\frac{2e^2n_e}{3m}\int_0^\infty\frac{u^{3/2}}{\nu_c-i\omega}\frac{df_0}{du}du. \tag{3}$$

Since both the total input power per unit column length and the electron density vary along the discharge, the left-hand side of Eq. (2), θ—the mean input power per electron—is also a function of the axial position z. This remark is important for the numerical procedure which is described in Sec. II D.

2. Heavy particle kinetics

The heavy particle kinetics includes a set of particle balance equations for all excited atoms considered as well as the balance equations for both atomic and molecular ions. The elementary processes taken into account with the corresponding references for the cross sections and rate constants data [40–53] are listed in Table I. The populations of excited atoms strongly depend on the radiation processes. The trapping of radiation is substantial not only for resonance, but also for the $4p$-$4s$ transitions, and it has been taken into account in all allowed radiative processes under consideration. The heavy particle kinetics is coupled with the electron kinetics in a self-consistent way in order to satisfy all balance equations and allows us to determine the atomic and molecular ion number densities as well as the populations of

TABLE I. Elementary processes included into the model and corresponding references for the cross sections and rate constants data.

Reaction	References
Elastic scattering	
$M+e \rightarrow M+e$, $M=e$, Ar^+, Ar_2^+	[42]
Excitation from ground state	
$Ar(^1S_0)+e \rightarrow Ar(m)+e$, $m=^3P_2$, $^3P_1$, $^3P_0$, $^1P_1$, $4p$	[40,42]
Excitation-deexcitation between excited states	
$Ar(m)+e \leftrightarrow Ar(n)+e$, $m,n=^3P_2$, $^3P_1$, $^3P_0$, $^1P_1$, $4p$	[41,43–46,52]
Ionization	
$Ar(m)+e \rightarrow Ar^+ +2e$, $m=^1S_0$, $^3P_2$, $^3P_1$, $^3P_0$, $^1P_1$, $4p$	[42,43]
Molecular ion formation	
$Ar^+ +2Ar \rightarrow Ar_2^+ +Ar$	[51]
Penning ionization	
$Ar(m)+Ar(m) \rightarrow Ar+Ar^+ +e$, $m=^3P_2$, $^3P_0$	[47]
Associative ionization	
$Ar(m)+Ar(m) \rightarrow Ar_2^+ +e$, $m=^3P_2$, $^3P_0$	[53]
Recombination	
$Ar_2^+ +e \rightarrow Ar(4p)+Ar$	[47]
$Ar^+ +e+e \rightarrow Ar(4p)+e$	[48]
Diffusion	
$M \rightarrow$ wall, $M=e$, Ar^+, Ar_2^+, $Ar(^3P_2)$, $Ar(^3P_0)$	[46,49]
Radiative processes	
$Ar(4p) \rightarrow Ar(m)+h\nu$, $m=^3P_2$, $^3P_1$, $^3P_0$, $^1P_1$	
$Ar(m) \rightarrow Ar+h\nu$, $m=^3P_1$, $^1P_1$	[50]

the excited states as a function of the electron number density. The full set of balance equations can be seen in [34].

As it has been outlined above, the model considers each level in the $4s$ block of levels separately and one lumped $4p$ block of levels. It is applicable at low and intermediate pressures (up to a few torrs) at degrees of ionizations up to 10^{-2} and provides sufficient accuracy for all plasma parameters.

3. Gas thermal balance equation

The local gas temperature can be found from the local gas thermal balance equation

$$-\frac{1}{r}\frac{d}{dr}\left(r\chi(r)\frac{dT_g^r}{dr}\right)=q_{\mathrm{ea}}(r)+q_{\mathrm{ei}}(r), \tag{4}$$

where $\chi(r)$ is the thermal conductivity being $\chi=4.17\times10^{-6}T_g^{r\,2/3}$ W cm^{-1} K$^{-5/3}$ for argon [54]. The terms on the right-hand side of Eq. (4), the power densities expended for gas neutral atoms' and ions' heating, are assumed to be proportional to the local electron density, $q_{\mathrm{ea/ei}}=q_{\mathrm{ea/ei}}(0)n_e(r)/n_e(0)$. The electron density radial profile is a Bessel-type with appropriate μ as we have already mentioned in Sec. II B 1. An accurate determination of the heating mechanism requires a detailed radial collisional–radiative model with precise calculation of the radial electron Boltzmann equation, which is beyond the scope of this paper. Equation (4) is solved under the boundary conditions $dT_g^r(0)/dr=0$ and $T_g^r(R)=T_w$. The gas temperature at the wall, T_w, has been assumed to be 300 K since in the gas-discharge conditions considered here the temperature of the discharge tube is practically equal to the room temperature [14]. The local T_g is

$$T_g=\frac{2}{R^2}\int_0^R rT_g^r(r)dr.$$

Since n_e varies along the plasma column length, T_g also changes in axial direction.

C. Surface-wave field equations

This part of the model considers Maxwell's equations for an azimuthally symmetric TM surface wave with field components $\mathbf{E}=(E_r,0,E_z)$ and $\mathbf{B}=(0,B_\varphi,0)$, where (r,φ,z) are the usual cylindrical coordinates. The wave propagates along

a plasma column (contained in a dielectric tube with a permittivity ε_d) in a setup with dimensions $2R$, $2R_d$, $2R_m$ (R being the plasma column radius, R_d the outer glass tube radius, and R_m the metal enclosure radius, respectively) and with a plasma permittivity ε_p,

$$\varepsilon_p = 1 - \frac{\omega_p^2}{\omega(\omega + i\nu_{\text{eff}})},$$

where $\omega_p = \sqrt{4\pi e^2 n_{\text{eff}}/m}$ is the electron plasma angular frequency and n_{eff} is the effective electron density [55]

$$n_{\text{eff}} = -\frac{2}{3}(\nu_{\text{eff}}^2 + \omega^2) n_e \int_0^\infty \frac{u^{3/2}}{\nu_c^2 + \omega^2} \frac{df_0}{du} du. \tag{5}$$

The effective electron-neutral collision frequency for momentum transfer

$$\nu_{\text{eff}} = \int_0^\infty \frac{\nu_c u^{3/2}}{\nu_c^2 + \omega^2} \frac{df_0}{du} du \Bigg/ \int_0^\infty \frac{u^{3/2}}{\nu_c^2 + \omega^2} \frac{df_0}{du} du \tag{6}$$

as well as n_{eff} have been introduced since for argon the electron-neutral collision frequency is energy dependent.

We consider the plasma as a weakly dissipative medium with an effective electron-neutral collision frequency for momentum transfer $\nu_{\text{eff}} < \omega$. In that case we can take $\varepsilon_p \sim 1 - \omega_p^2/\omega^2$. Following for simplicity an assumption for radially averaged electron and excited atom densities and using as boundary conditions the continuity of electric and magnetic field tangential components (or equality of plasma, dielectric, and vacuum impedances) at the interfaces, one can derive the local wave dispersion relation. In particular, for the aforementioned setup the local dispersion relation gets the form [12]

$$\frac{\varepsilon_p}{a_p} \frac{I_1(a_p)}{I_0(a_p)} + \frac{\varepsilon_d}{a_d} \frac{\alpha_1 + a_d \alpha_2 \Delta/\varepsilon_d a_v}{\alpha_3 + a_d \alpha_4 \Delta/\varepsilon_d a_v} = 0, \tag{7}$$

where

$$a_p = (x^2 - \sigma^2 \varepsilon_p)^{1/2}, \quad a_d = (\sigma^2 \varepsilon_d - x^2)^{1/2},$$

$$a_v = (x^2 - \sigma^2)^{1/2}, \quad \sigma = \omega R/c, \quad x = kR,$$

$$\alpha_1 = J_1(a_d) H_1^{(1)}(a_d\gamma) - J_1(a_d\gamma) H_1^{(1)}(a_d),$$

$$\alpha_2 = J_1(a_d) H_0^{(1)}(a_d\gamma) - J_0(a_d\gamma) H_1^{(1)}(a_d),$$

$$\alpha_3 = J_1(a_d\gamma) H_0^{(1)}(a_d) - J_0(a_d) H_1^{(1)}(a_d\gamma),$$

$$\alpha_4 = J_0(a_d\gamma) H_0^{(1)}(a_d) - J_0(a_d) H_0^{(1)}(a_d\gamma).$$

$$\Delta = \frac{K_1(a_v\gamma) + I_1(a_v\gamma) K_0(a_v\eta)/I_0(a_v\eta)}{K_0(a_v\gamma) - I_0(a_v\gamma) K_0(a_v\eta)/I_0(a_v\eta)}.$$

Here $\gamma = R_d/R$, $\eta = R_m/R$, c is the speed of light, k is the wave number, and J_0, J_1 are the Bessel functions, I_0, I_1, K_0, K_1 the modified Bessel functions, and $H_0^{(1)}$, $H_1^{(1)}$ the Hankel functions of zeroth and first order, respectively. The local dispersion equation yields, for a given axial position z, a relation between the electron density (n_{eff} or n_e) and the wave number k—the so-called phase diagram.

From Poynting's theorem one gets another important equation which reads

$$\frac{dS}{dz} = -Q, \tag{8}$$

where S is the wave energy flux, being a sum of the axial components of Poynting's vector averaged over the wave period $2\pi/\omega$ and integrated over the plane normal to the plasma column, from the axis to the metal screen radius, at a given axial position z:

$$S = 2\pi \int_0^R r S_z^p \, dr + 2\pi \int_R^{R_d} r S_z^d \, dr + 2\pi \int_{R_d}^{R_m} r S_z^v \, dr. \tag{9}$$

Here p, d, and v denote plasma, dielectric and vacuum, respectively, and for an azimuthally symmetric wave the longitudinal component of Poynting's vector is

$$S_z = \frac{c}{8\pi} \text{Re}(E_r^* B_\varphi).$$

An explicit expression of S for the setup under consideration can be found in [12,17].

In the wave energy balance Eq. (8), Q is the wave power per unit column length absorbed by electrons,

$$Q = 2\pi \int_0^R r \langle \mathbf{j} \cdot \mathbf{E} \rangle dr = \frac{1}{8} \frac{\overline{n_e}}{n_{\text{cr}}} \nu_{\text{eff}} R^2 E_0^2, \tag{10}$$

where now $\langle\ \rangle$ means averaging over the wave period, $\overline{n_e} \equiv n_e$ is the radially averaged electron density, $n_{\text{cr}} = m\omega^2/4\pi e^2$, and

$$E_0^2 = \frac{2}{R^2} \int_0^R r |\mathbf{E}|^2 \, dr \tag{11}$$

is the radially averaged squared wave electric field which can be expressed in terms of the axial wave electric field component at the plasma-dielectric interface, $E_z(R) \equiv E$, and modified Bessel functions, i.e.,

$$E_0^2 = E^2 \left[1 - \frac{I_1^2(a_p)}{I_0^2(a_p)} - \frac{x^2}{a_p^2} \left(1 - \frac{I_1^2(a_p)}{I_0^2(a_p)} - \frac{2}{a_p} \frac{I_1(a_p)}{I_0(a_p)} \right) \right].$$

On the other hand, Q is the power expended by electrons in elastic and inelastic collisions and it can be presented in the form

$$Q = \pi R^2 n_e \theta. \tag{12}$$

From both equations for Q with values of θ and ν_{eff} calculated in the kinetic part the squared wave electric field, E_0^2 can be presented in the form

$$E_0^2 = \frac{2m}{e^2} \frac{n_e}{n_{\text{eff}}} \frac{\nu_{\text{eff}}^2 + \omega^2}{\nu_{\text{eff}}} \theta.$$

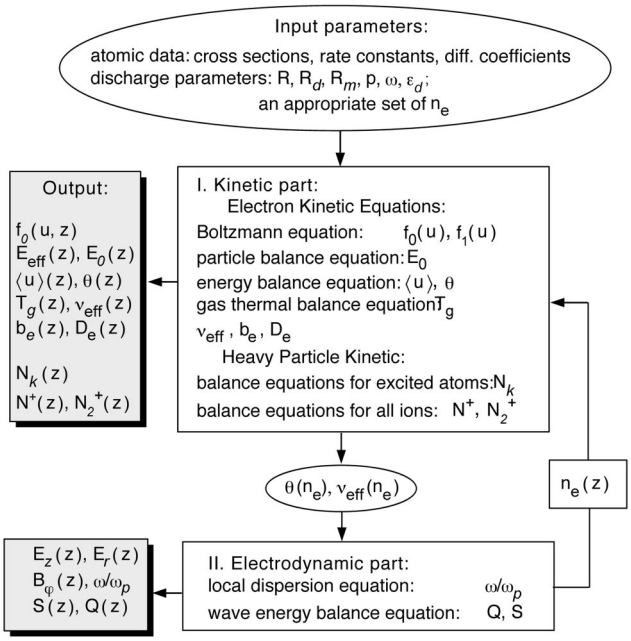

FIG. 2. Algorithm of the numerical calculations.

This expression for E_0^2 enters [via Eq. (10)] into Eq. (8), which solved together with the local dispersion relation (7) yields the axial distribution of all plasma column and wave characteristics. Recall that in most of our previous modelings of plasma columns sustained by SWs there were used normalized quantities [5,17]. In particular, the normalization of the axial position z included the usage of $\nu_{\rm eff}$, of the wave energy flux S (in fact, the wave power sustaining the discharge)—the mean power θ, and of all wave field components E_r, E_z, B_φ—both $\nu_{\rm eff}$ and θ. To compare, for example, the column length $z_{\rm column}$ or the power S necessary to sustain it, one had to introduce reliable values for $\nu_{\rm eff}$ and θ (calculated separately or taken from experimental data). Thus those modelings were, in general, not self-contained. Moreover, the connection between θ and n_e was set to be in the form $\theta \propto n_e^{1+\beta}$ with an appropriate constant β—$\beta=0$ for diffusion-controlled discharges and $0<\beta\leqslant 2$ for recombination regimes (that relation was extracted from the electron energy balance equation)—and to be independent of the axial position. In fact, such a relation between θ and n_e was necessary because there was no true kinetic part in that model.

D. Numerical procedure

A self-consistent treatment becomes possible after coupling the kinetic and electrodynamic parts through the electron energy balance equation. The basic concept of the numerical calculations is presented schematically in Fig. 2. The description of the numerical algorithm is given in detail below.

In order to initialize the electrodynamic equations, numerical solutions to the electron Boltzmann Eq. (1) coupled with the balance equations for all species involved have been performed in the expected interval of electron densities (10^{10}–10^{15} cm^{-3}). Once the dependence of E_0, $\nu_{\rm eff}$, and θ on the electron density n_e is obtained, the electrodynamic equations can be solved. The local dispersion relation (7) yields for a given wave number k the electron density n_e, and the solution to the wave energy balance Eq. (8) provides the dependence of the electron density on the axial position z, i.e., $n_e(z)$. Equation (8) is a first-order differential equation and requires one boundary condition. In our numerical code either the total input power delivered to the discharge or the electron density at the wave exciter can be used as a boundary condition for Eq. (8). Having obtained the axial dependence of the electron density $n_e(z)$, the kinetic part is recalculated again for appropriate axial positions. This provides the spatial evolution of the isotropic distribution function, mean electron energy, transport parameters, gas temperature, fractional particle and power gain and loss, various rate constants for electron–heavy particle collisional processes, and the axial distribution of atomic and molecular ions alongside the populations of the excited states.

Due to its modular structure, the model can be easily adapted to different discharge configurations or other gases. The flexibility of the model enables one to involve many plasma components as well as a wide range of reactions in each plasma component.

III. RESULTS AND DISCUSSION

A. Comparison with experimental data

The results presented below illustrate the applicability of the model to a wide range of discharge conditions. A comparison between the modeling and two typical experiments for an argon plasma column sustained by a SW will be discussed, namely that of Darchicourt *et al.* [56] with the following vessel parameters: cross section $\varnothing=76$, 80, and 190 mm, dielectric permittivity $\varepsilon_d=4.0$, wave frequency $\omega/2\pi=390$ MHz, gas pressure of 250 mTorr, and as an input parameter the electron number density at the exciter $n_{e0}=3\times10^{10}$ cm^{-3} and that of Boisse-Laporte *et al.* [7] with vessel parameters $\varnothing=4$, 8, and 40 mm, dielectric permittivity $\varepsilon_d=4.0$ and microwave frequency $\omega/2\pi=2.45$ GHz at gas pressure of 1 Torr with input parameter the power at the exciter being $S_0=300$ W.

The axial variation of the EEDF is plotted in Fig. 3. For both experiments the EEDF has a non-Maxwellian character. The axial variation of the distribution function is due to several factors. The amplitude of the local EEDF decreases in axial direction because of a decrease in the local electron density while the EEDF profiles for different axial positions change as a result of electron-electron collisions. For the first of the chosen experiments (with degree of ionization of 10^{-6}), an increase of the EEDF in the low-energy part can be observed. This typical shape of the EEDF at similar discharge conditions has been obtained and widely discussed in [13,35,57]. For the second experiment (where the degree of ionization is 10^{-3}) the tip in the local EEDF at low kinetic energy is absent because of the impact of electron-electron collisions.

In Figs. 4 and 5 the experimental data are compared with the results of the numerical calculations—those for the first experiment on the left sides of the figures and for the second on the right sides, respectively. The common tendency of decreasing in axial direction of both the electron number density n_e and the wave power S necessary to sustain the rest of

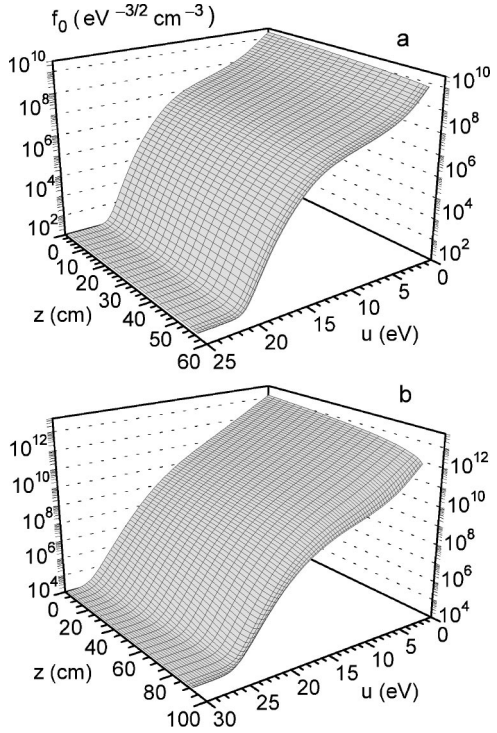

FIG. 3. Axial variation of the EEDF for (a) an electromagnetic wave of frequency $\omega/2\pi=390$ MHz, vessel parameters $\varnothing=76, 80, 190$ mm, $\varepsilon_d=4.0$ at gas pressure of 250 mTorr; and (b) for $\omega/2\pi=2.45$ GHz, $\varnothing=4, 8, 40$ mm, $\varepsilon_d=4.0$ at gas pressure of 1 Torr.

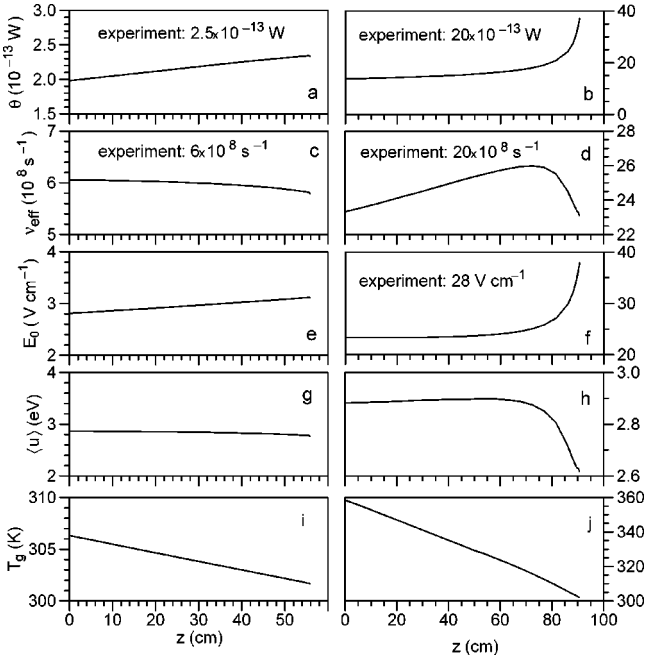

FIG. 5. The mean power θ required for sustaining an electron-ion pair in the discharge (a) and (b), effective electron-neutral collision frequency for momentum transfer ν_{eff} (c) and (d), maintenance wave electric field E_0 (e) and (f), mean electron energy $\langle u\rangle$ (g) and (h), and gas temperature T_g (i) and (j) as functions of the axial position z. The discharge conditions are the same as in Fig. 3(a) for (a), (c), (e), (g), and (i) and as those in Fig. 3(b) for (b), (d), (f), (h), and (j).

the plasma column is easily seen—S equals zero at the column end. The experimental data plotted with filled squares in Fig. 4(a) are for a homogeneous radial plasma density profile $[n_e(r)=\text{const}]$ with $\mu=0$ while those with open squares are for a heterogeneous profile with $\mu=2.15$ [56]. In our calculations we have assumed a radial profile with $\mu=2.15$ for the first experiment and $\mu=2.405$ for the second one. Since the

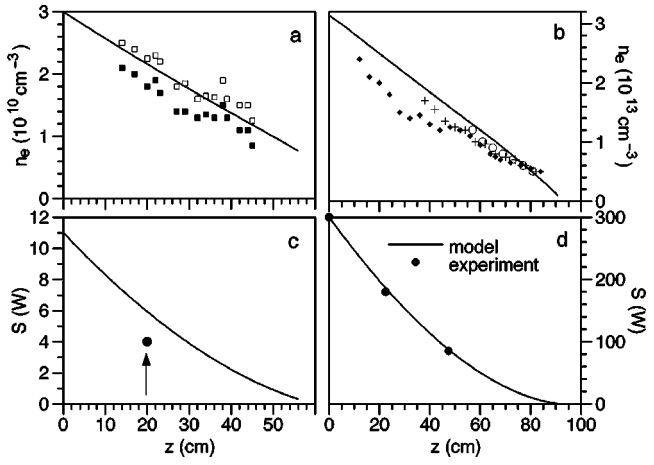

FIG. 4. Electron densities (a) and (b) and wave energy fluxes (c) and (d) axial profiles. Experimental data: (a) full squares for $\mu=0$ and open squares for $\mu=2.15$; (b) full diamond suits with $\mu=2.405$ for input power of 300 W, pluses for 180 W, and open circles for 85 W; (c) and (d) the bullets show the absorbed wave power. The discharge conditions are the same as in Fig. 3(a) for (a) and (c) and as those in Fig. 3(b) for (b) and (d).

radial electron density profile influences the determination of discharge characteristics, this circumstance emphasizes the necessity of a strict calculation of the radial EEDF [58], especially for small pR. Our numerical modeling nonetheless fits very well the experimental data. Note that the wave powers measured experimentally [plotted with bullets in Figs. 4(c) and 4(d)] lay very close to the calculated theoretical curves for both experiments. The agreement between measured and calculated n_e is good.

Having obtained the axial variation of the EEDF, the axial profiles of all discharge characteristics, namely θ, ν_{eff}, the wave electric field E_0, the mean electron energy $\langle u\rangle$, the gas temperature T_g, as well as the densities of excited states, atomic and molecular ions are calculated and plotted in Figs. 5–7. For the gas pressure of 250 mTorr the axial course of all curves in Fig. 5 is almost linear while for the pressure of 1 Torr it is strongly nonlinear at the column end except the $T_g(z)$ dependence. The available experimental data are also presented in the same figure. The discrepancies between model and experiment are less than 20%. The partial contribution of several groups of elementary processes included in θ is shown in Fig. 6. The excitation, the direct and stepwise ionization, and the diffusion and dissociative recombination have been included in the energy loss of electrons while the heating from the wave electric field, the deexcitaion, the Penning, and the associative ionizations have been taken into account as an electron energy gain in Eq. (2). For both experiments the main loss mechanism is the electron impact excitation. For convenience, the energy gain through deexcitation is subtracted from the energy loss by excitation and, in

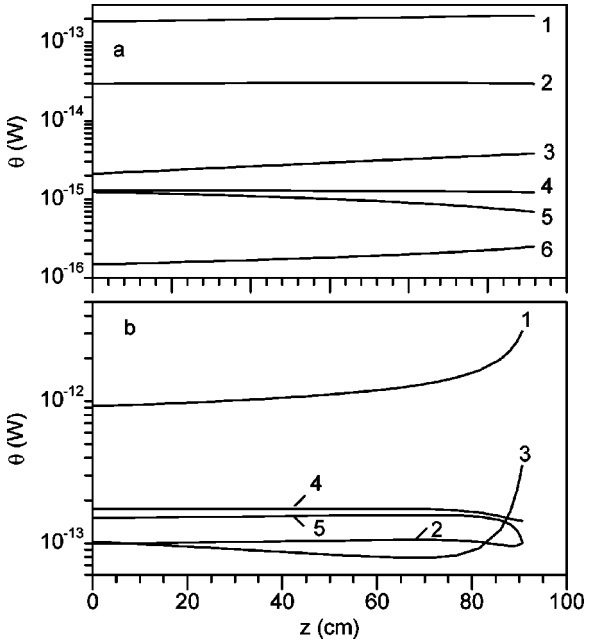

FIG. 6. Partial contribution of 1—excitation–deexcitation, 2—elastic collisions, 3—direct ionization, 4—diffusion, 5—stepwise ionization, and 6—Penning ionization (negative contribution) to the electron power loss, θ, for the same discharge conditions as in Fig. 3(a) and Fig. 3(b), respectively.

fact, the net energy loss is plotted. Figure 7 shows the population of the excited states and the densities of atomic and molecular ions. For the first experiment (at the 250 mTorr gas pressure) the populations of the $4s$ states slightly decrease when going from the exciter towards the plasma column end while for the gas pressure of 1 Torr they increase. This observation indicates that there are different creation–loss mechanisms for the excited states in the two discharges. For the first experiment the population of the $4p$ block of levels is one-thousandth of the population of the $4s$ levels while for the second one that population is comparable with the populations of the $4s$ levels' block. Thus the importance of including the $4p$ block of levels in our model, especially

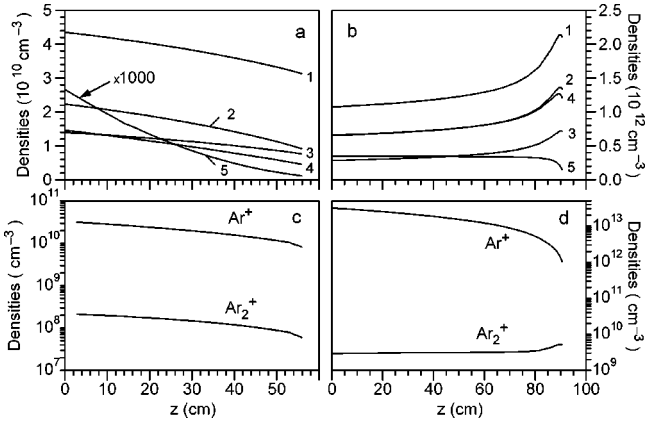

FIG. 7. Populations of the excited states (a) and (b) and densities of Ar^+ and $Ar_2{}^+$ (c) and (d). The curve 1 denotes $^3P_2$, the curve 2—$^3P_1$, the curve 3—$^3P_0$, the curve 4—$^1P_1$, and 5—$4p$ block of levels. The discharge conditions are the same as in Fig. 3(a) for (a) and (c) and as those in Fig. 3(b) for (b) and (d).

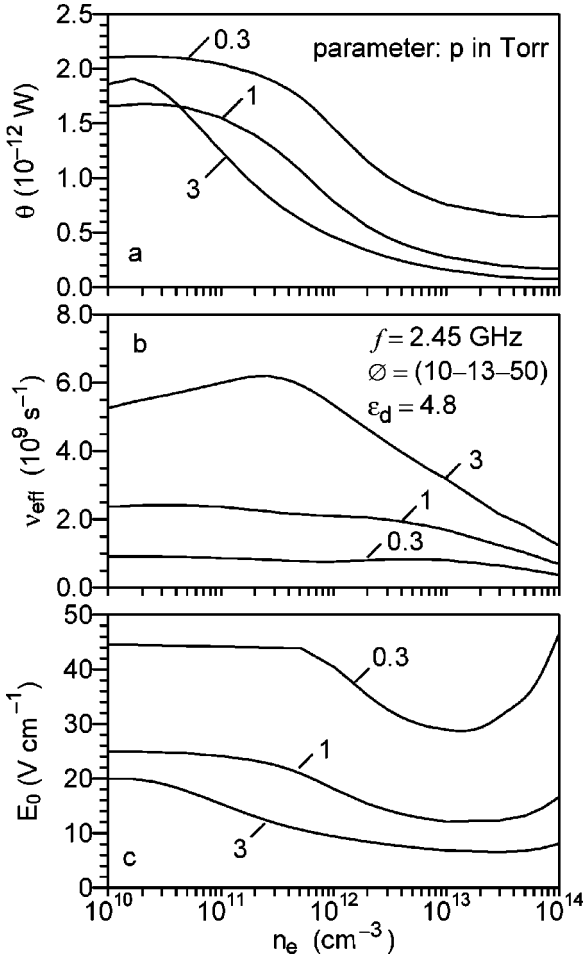

FIG. 8. The power absorbed by electrons θ, the effective electron-neutral collision frequency for momentum transfer ν_{eff}, and the maintenance electric field E_0 as a function of the electron number density at various gas pressures. The vessel parameters are $\varnothing = 10, 13, 50$ mm, $\varepsilon_d = 4.8$, and the wave frequency is 2.45 GHz.

at high electron densities, becomes obvious. From Figs. 7(c) and 7(d) it can be seen that for both experiments the Ar^+ is the dominant ion in plasmas. The molecular $Ar_2{}^+$ ion which is less than 1% of the total ion density is considered in order to account for eventual recombination losses at higher electron densities or gas pressures.

B. Influence of the gas pressure on the plasma column characteristics

In this subsection, the results of a theoretical investigation of plasma sustained by a traveling electromagnetic wave at various gas pressures are reported. In particular, for vessel parameters $\varnothing = 10$, 13, and 50 mm, dielectric permittivity $\varepsilon = 4.8$, and wave frequency $f = 2.45$ GHz we investigate the discharge characteristics when changing the gas pressure from 0.3 to 3 Torr. The dependences of θ, ν_{eff}, and E_0 on the electron number density, n_e, are plotted in Fig. 8. Figure 9 shows the gas temperature as a function of n_e. Note that in the two figures the electron density is in a logarithmic scale. It is seen from Fig. 8(a) that the change of θ at high electron densities is negligible at all pressures, however for n_e in the interval of 10^{11}–10^{13} cm^{-3} that variation is substantial and more pronounced at higher gas pressures. Figure 8(b) sug-

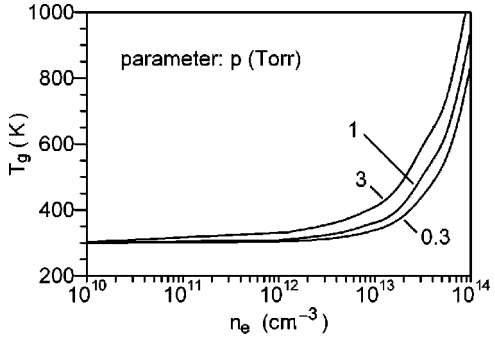

FIG. 9. Gas temperature as a function of the electron number density. The discharge conditions are the same as in Fig. 8.

gests that at low gas pressures the effective collision frequency for momentum transfer, ν_{eff}, can be accepted as a constant. At low gas pressures and relatively low plasma densities—the usual case at laboratory experiments—the wave electric field is also practically constant as Fig. 8(c) shows. According to Fig. 9, the gas temperature is practically constant at $n_e < 10^{12}$ cm^{-3}; however, it changes significantly at higher electron densities. This means that in that case the variation of the gas temperature along the column length has to be taken into account. The axial distribution of the electron density and the wave power is depicted in Fig. 10 for plasma columns sustained by a 100 W input power. With increasing the gas pressure, plasma density and column length increase, too. The axial profiles of θ and ν_{eff} are plotted in Fig. 11. For a gas pressure above approximately 1 Torr, they are not constant as it was assumed in previous works. Both θ and ν_{eff} increase at the plasma column end. This was observed experimentally by Lao *et al.* [59] for gas pressures of 1.2 and 3.5 Torr; however, the authors considered θ and ν_{eff} as independent of the axial position.

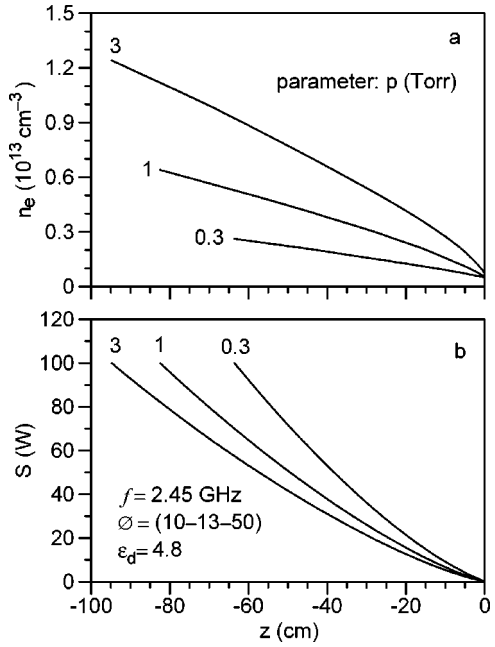

FIG. 10. Electron density (a) and wave energy flux (b) axial profiles at various gas pressures. The discharge conditions are the same as in Fig. 8. For convenience z is set from the column end.

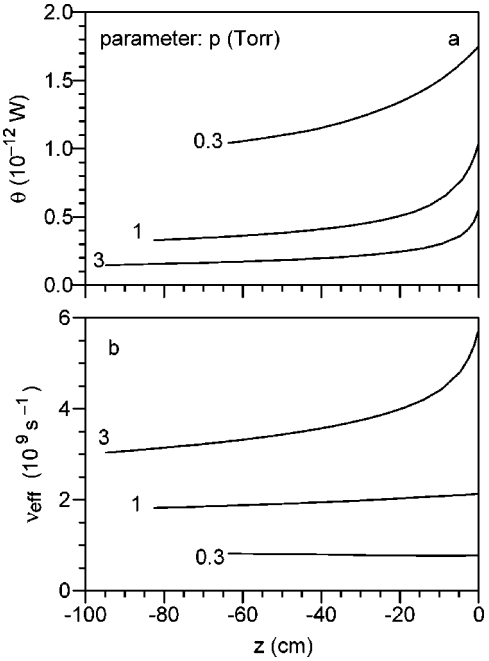

FIG. 11. The absorbed power per electron θ (a) and the effective electron-neutral collision frequency for momentum transfer ν_{eff} (b) at various gas pressures. The conditions are the same as denoted in Fig. 10(b). For convenience z is set from the column end.

The plasma column length depends essentially on the energy loss of electrons. In order to understand the energy loss mechanism, the partial contributions of different groups of elementary processes included in θ have been investigated. The results for various pressures and axial positions are presented in Table II.

The axial dependence of the mean energy, mobility, and diffusion coefficient for electrons is plotted in Fig. 12. At pressures below 1 Torr the mean electron energy [Fig. 12(a)] is almost constant along the plasma column, while at higher gas pressures it changes due to the axial variation of the local EEDF. The results for axial dependence on the electron mobility b_e and the electron diffusion coefficient D_e at different gas pressures are presented in the figure below. As in Fig. 12(a), the axial variation of both b_e and the D_e is pronounced above 1 Torr gas pressure. It can be attributed to the change of both the neutral atom density (which depends on the axial variation of T_g) and the local EEDF.

Figure 13(a) presents the axial distribution of the wave electric field E_0 which shows a general tendency to increase near the column end and to decrease with the growing of the gas pressure. New theoretical results for the axial distribution of the gas temperature T_g as a function of the gas pressure are illustrated in Fig. 13(b). To the best of our knowledge, there are no experimental results for gas-temperature axial variations in microwave argon discharges to compare with our theoretical curves. Such measurements have been performed in a nitrogen SW sustained plasma [60] and the axial course of the gas temperature is similar to ours (see Fig. 2 in Ref. [60])—the absolute values of the temperatures are of course different because of the different gas nature and gas-discharge conditions. The temperature of the neutral gas decreases from the wave launcher towards the column end due to the decrease of n_e and this decrease is more distinc-

TABLE II. Partial contribution of the elementary processes in the electron power loss at various gas pressures, axial positions, and gas-discharge conditions as in Fig. 10(b).

Partial power loss	Pressure (Torr)	Axial position (cm) 0	20	40	60	80	end
	0.3	1.40	0.98	0.85			0.71
Elastic	1	6.17	5.84	5.48	3.88		2.78
collisions	3	20.62	20.41	19.75	19.31	18.10	16.07
	0.3	77.38	78.77	79.74			82.47
Excitation-	1	82.44	83.57	84.57	88.09		91.38
deexcitation	3	72.66	73.28	74.42	75.40	77.26	80.79
	0.3	7.61	8.17	9.93			15.01
Direct	1	0.88	0.81	0.75	0.73		2.45
ionization	3	0.09	0.07	0.05	0.03	0.02	0.01
	0.3	6.28	5.53	4.15			1.79
Stepwise	1	5.82	5.43	4.91	4.10		1.77
ionization	3	4.04	3.78	3.49	3.19	2.76	1.83
Penning and	0.3	−0.01	−0.01	−0.01			−0.02
associative	1	−0.02	−0.03	−0.03	−0.05		−0.02
ionization	3	−0.01	−0.01	−0.01	−0.02	−0.02	−0.02
	0.3	7.34	6.56	5.34			0.04
Diffusion	1	4.69	4.36	4.30	3.24		1.63
	3	2.37	2.25	2.08	1.91	1.71	1.23
	0.3	0.00	0.00	0.00			0.00
Dissociative	1	0.02	0.02	0.02	0.01		0.01
recombination	3	0.23	0.22	0.22	0.18	0.17	0.09

tive at higher pressures where the gas temperature itself is, in general, higher. The widely used assumption for a constant gas temperature of around 300 K is obviously applicable only at gas pressures below 1 Torr. The proper account of T_g is essential since it affects the neutral atom density. The latter is important for a correct calculation of ν_{eff}, E_0, and θ, which are input parameters in the electrodynamic part. Omitting the gas temperature dependence can lead to errors in calculating the axial discharge structure and electrodynamic properties of the weakly ionized plasma and in particular in determining the plasma column length.

IV. CONCLUSION

In this paper, the axial structure of a plasma column sustained by a traveling electromagnetic wave has been investigated. The axial variation of the EEDF calculated numerically from the electron Boltzmann equation together with the heavy particle kinetics and gas thermal equation is coupled self-consistently with the local dispersion relation and the wave energy balance equation. As a result of the numerical procedure, the axial profiles of the electron density, the wave power, the maintaining electric field, the gas temperature, the mean electron energy, the electron mobility, the atomic and molecular ions' densities, as well as the populations of all excited states have been obtained in a wide range of dis-

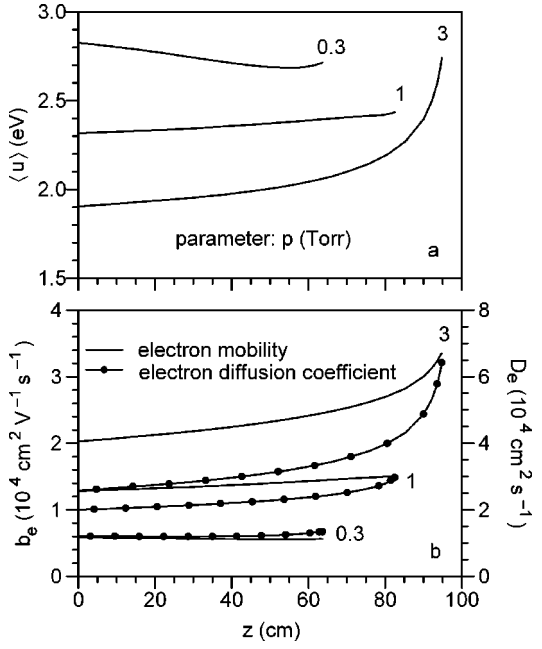

FIG. 12. Axial distributions of the mean energy $\langle u \rangle$ (a) and electron mobility b_e and diffusion coefficient D_e (b) at different gas pressures. The conditions are the same as in Fig. 10(b).

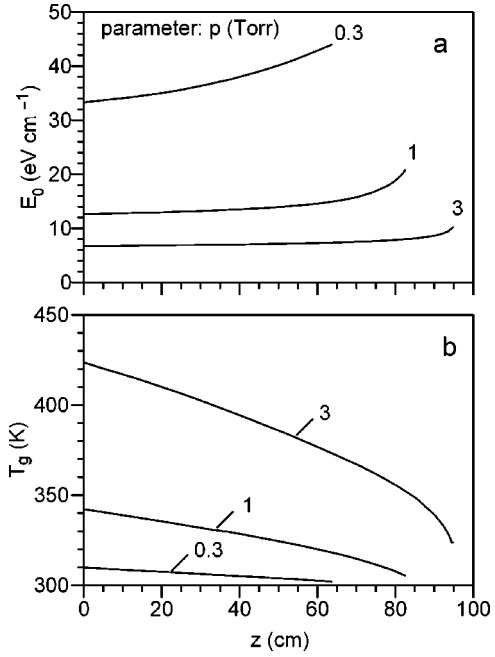

FIG. 13. Axial distribution of the maintenance electric field E_0 (a) and gas temperature T_g (b) at various gas pressures. The conditions are as denoted in Fig. 10(b).

charge conditions: wave frequency of 390 MHz and 2.45 GHz, plasma column radius of 0.2 cm and 3.8 cm, gas pressures from 0.25 to 3 Torr. The comparison between theory and experiment shows good agreement.

The model presented here has several advantages compared to our previous investigations (see, for example, [17]).

(i) The postulated connection between the absorbed wave power per unit column length and the radially averaged electric field intensity based on supposed creation-loss mechanisms of the charged particles and different discharge regimes has been avoided by taking into consideration a collisional-radiative model for the argon plasma.

(ii) In our previous models the axial profiles of the wave and plasma column characteristics have been obtained in normalized quantities, and for comparison with available experimental profiles imported outside the model values of θ and ν_{eff} very often have been used. The knowledge of the real axial profile of the latter plasma parameters is of fundamental importance. It allows one to obtain the axial structure of the wave electric and magnetic field components and the wave power in absolute units. Moreover, θ and ν_{eff} are found to be axially dependent at gas pressures above 1 Torr. They can be obtained only by a strict kinetic modeling. This leads to a substantial improvement of the whole electrodynamic part of the model.

(iii) From our model the space-dependent behavior of several plasma characteristics can be derived, namely, the mean energy and mobility of electrons, the maintenance wave electric field, and the particle densities.

(iv) The gas temperature, whose magnitude has been fixed in all works up to now, in the frame of our model is obtained self-consistently and it turns out to be not constant along the column length. The gas temperature decreases from the wave launcher towards the column end and this decrease is prominent especially at higher pressures.

(v) Since the model can predict both the wave and plasma characteristics, an optimization of experiments can be done.

A weakness of the present model is that the actual radial structure has not been taken into account. Another limitation of our model is the requirement $\nu_{\mathrm{eff}} < \omega$. The latter comes from the electrodynamic part and further development in the modeling of the surface wave discharges at intermediate gas pressures has to avoid this limitation.

ACKNOWLEDGMENTS

The authors would like to thank Professor C. M. Ferreira and Professor R. Winkler for valuable and stimulating discussions. This work was supported by the National Fund for Scientific Research under Grant No. F-821/98.

[1] V. M. M. Glaude, M. Moisan, R. Pantel, P. Leprince, and J. Marec, J. Appl. Phys. **51**, 5693 (1980).
[2] C. M. Ferreira, J. Phys. D **14**, 1811 (1981); **16**, 1673 (1983).
[3] Z. Zakrzewski, J. Phys. D **16**, 171 (1983).
[4] E. Mateev, I. Zhelyazkov, and V. Atanassov, J. Appl. Phys. **54**, 3049 (1983).
[5] I. Zhelyazkov, E. Benova, and V. Atanassov, J. Appl. Phys. **59**, 1466 (1986).
[6] C. M. Ferreira, in *Radiative Processes in Discharge Plasmas*, edited by J. M. Proud and L. H. Luessen (Plenum, New York, 1986), p. 431.
[7] C. Boisse-Laporte, A. Granier, E. Dervisevic, P. Leprince, and J. Marec, J. Phys. D **20**, 197 (1987).
[8] C. M. Ferreira and M. Moisan, Phys. Scr. **38**, 382 (1988).
[9] I. Zhelyazkov and E. Benova, J. Appl. Phys. **66**, 1641 (1989).
[10] C. M. Ferreira, J. Phys. D **22**, 705 (1989).
[11] C. M. Ferreira, in *Nonequilibrium Processes in Partially Ionized Gases*, edited by M. Capitelli and J. N. Bardsley (Plenum, New York, 1990), p. 187.
[12] E. Benova and I. Zhelyazkov, Phys. Scr. **43**, 68 (1991).
[13] U. Kortshagen, H. Schlüter, and A. Shivarova, J. Phys. D **24**, 1571 (1991).
[14] A. B. Sá, C. M. Ferreira, S. Pasquiers, C. Boisse-Laporte, P. Leprince, and J. Marec, J. Appl. Phys. **70**, 4147 (1991).
[15] Yu. M. Aliev, K. M. Ivanova, M. Moisan, and A. Shivarova, Plasma Sources Sci. Technol. **2**, 145 (1993).
[16] C. M. Ferreira, in *Microwave Discharges: Fundamentals and Applications*, edited by C. M. Ferreira and M. Moisan (Plenum, New York, 1993), p. 313.
[17] I. Zhelyazkov and V. Atanassov, Phys. Rep. **255**, 79 (1995).
[18] X. L. Zhang, F. M. Dias, and C. M. Ferreira, Plasma Sources Sci. Technol. **6**, 29 (1997).
[19] M. Moisan, Z. Zakrzewski, and R. Pantel, J. Phys. D **12**, 219 (1979).
[20] M. Moisan, Z. Zakrzewski, R. Pantel, and P. Leprince, IEEE Trans. Plasma Sci. **12**, 203 (1984).
[21] M. Moisan and Z. Zakrzewski, Rev. Sci. Instrum. **58**, 1895 (1987).

[22] Z. Zakrzewski and M. Moisan, Plasma Sources Sci. Technol. **4**, 379 (1994).
[23] J. Margot-Chaker, M. Moisan, V. M. M. Glaude, P. Lauque, J. Paraszczak, and G. Sauvé, J. Appl. Phys. **66**, 4134 (1989).
[24] E. Benova, I. Ghanashev, and I. Zhelyazkov, J. Plasma Phys. **45**, 137 (1991).
[25] M. Djourelova, Ts. Petrova, I. Ghanashev, and I. Zhelyazkov, J. Phys. D **26**, 1601 (1993).
[26] I. Zhelyazkov, E. Benova, and V. Atanassov, J. Appl. Phys. **62**, 2713 (1987).
[27] S. Pasquiers, C. Boisse-Laporte, A. Granier, E. Bloyet, P. Leprince, and J. Marec, J. Appl. Phys. **65**, 1465 (1989).
[28] E. Benova, I. Zhelyazkov, P. Staikov, and F. Cap, Phys. Rev. A **44**, 2625 (1991).
[29] J. Margot and M. Moisan, in *Microwave Discharges: Fundamentals and Applications*, edited by C. M. Ferreira and M. Moisan (Plenum, New York, 1993), p. 141.
[30] M. Djourelova, I. Zhelyazkov, and I. Ghanashev, Plasma Phys. Controlled Fusion **36**, 1355 (1994).
[31] I. Pérès, M. Fortin, and J. Margot, Phys. Plasmas **3**, 1754 (1996).
[32] I. Pérès and J. Margot, Plasma Sources Sci. Technol. **5**, 653 (1996).
[33] I. Pérès, A. Dallaire, P. Jones, and J. Margot, J. Appl. Phys. **82**, 4211 (1997).
[34] E. Benova, Ts. Petrova, A. Blagoev, and I. Zhelyazkov, J. Appl. Phys. **84**, 147 (1998).
[35] U. Kortshagen, in *Microwave Discharges: Fundamentals and Applications*, edited by C. M. Ferreira and M. Moisan (Plenum, New York, 1993), p. 303.
[36] R. Winkler, M. Capitelli, M. Dilorando, C. Gorse, and J. Wilhelm, Plasma Chem. Plasma Process. **6**, 437 (1986).
[37] S. Yoshida, A. V. Phelps, and L. C. Pitchford, Phys. Rev. A **27**, 2858 (1983).
[38] M. Moisan, C. M. Ferreira, Y. Hajlaoui, D. Henry, J. Hubert, R. Pantel, A. Ricard, and Z. Zakrzewski, Rev. Phys. Appl. **17**, 707 (1982).
[39] D. Loffhagen and R. Winkler, J. Comput. Phys. **112**, 91 (1994).
[40] J. Vlček, J. Phys. D **22**, 626 (1989).
[41] H. W. Drawin, Z. Phys. **225**, 483 (1969).
[42] M. Hayashi (private communication).
[43] L. Vriens and A. M. Smeets, Phys. Rev. A **22**, 940 (1980).
[44] I. Yu. Baranov, V. I. Demidov, and N. B. Kolokolov, Opt. Spektrosk. **51**, 316 (1981) [Opt. Spectrosc. **51**, 173 (1981)].
[45] I. Yu. Baranov, V. I. Demidov, and N. P. Penkin, Opt. Spektrosk. **58**, 268 (1985) [Opt. Spectrosc. **58**, 160 (1985)].
[46] E. W. McDaniel, *Collision Phenomena in Ionized Gases* (Wiley, New York, 1964).
[47] T. Okada and M. Shugawara, J. Phys. D **26**, 1680 (1993).
[48] L. M. Biberman, V. S. Vorob'ov, and I. T. Iakubov, *Kinetics of Non-Equilibrium Low-Temperature Plasma* (Plenum, New York, 1987).
[49] C. M. Ferreira, J. Loureiro, and A. Ricard, J. Appl. Phys. **57**, 82 (1985).
[50] T. Holstein, Phys. Rev. **72**, 1212 (1947); **83**, 1195 (1951).
[51] J. D. C. Jones, D. G. Lister, D. P. Wareing, and N. D. Twiddy, J. Phys. B **13**, 3247 (1980).
[52] A. Hyman, Phys. Rev. A **18**, 441 (1978); **24**, 1094 (1981).
[53] N. B. Kolokolov, A. A. Kudryavtsev, and A. B. Blagoev, Phys. Scr. **50**, 371 (1996).
[54] Yu. B. Golubovskii and R. Sonneburg, Zh. Tekh. Fiz. **49**, 295 (1979) [Sov. Phys. Tech. Phys. **24**, 173 (1979)].
[55] F. Whitmer and G. F. Herrmann, Phys. Fluids **9l**, 768, (1966).
[56] R. Darchicourt, S. Pasquiers, C. Boisse-Laporte, P. Leprince, and J. Marec, J. Phys. D **21**, 293 (1988).
[57] U. Kortshagen and H. Schlüter, J. Phys. D **24**, 1585 (1991).
[58] D. Uhrlandt and R. Winkler, Plasma Chem. Plasma Process. **16**, 517 (1996).
[59] C. Lao, J. Cotrino, A. Sola, A. Gamero, M. T. Benavides, M. Saez, M. D. Caldaza, and V. Colomer, in *ESCAMPIG 88 Abstracts of Invited Talks and Contributed Papers*, edited by C. M. Ferreira (European Physical Society, Geneva, 1988), p. 171.
[60] E. Tatarova, F. M. Dias, C. M. Ferreira, and A. Ricard, J. Appl. Phys. **85**, 49 (1999).